Theoret. Appl. Mech., Vol.37, No.2, pp.111-137, Belgrade 2010

Spectral analysis of nonlinear systems

Sandy Black* **David Christie†**
Neil Finlayson†

Abstract

Two separate nonlinear differential systems are investigated in the frequency and time domains using plots generated by Mathematica. Spectral density plots are of particular interest as they can conveniently demonstrate the effect on a system of changing one of the parameters. The effects of the starting displacement on the nonlinear pendulum, and the behaviour of the Lorenz system when the Rayleigh number is varied, are considered in this way.

Keywords: Nonlinearity, spectral, Lorenz

1 Introduction

Systems of nonlinear differential equations play an important part in subjects as diverse as meteorology, oceanography, optics, economics and biology. Understanding nonlinear behaviour is also required for renewable energy engineering, including modelling the wave and

*Glasgow University, Glasgow, G12 8QQ, UK. Research conducted during summer placement at Greenspace Research.

†Greenspace Research, Lews Castle College UHI, Stornoway, Isle of Lewis HS2 0XR, UK

tidal power resource, and developing novel methods of harvesting energy with wave-driven pendulums [6]. Such dynamical systems are rarely amenable to exact analytical solution, and numerical modelling is frequently required to supplement experimental research.

Nonlinear systems are found to exhibit a rich variety of behaviour, including chaos. Many interesting features of such systems can be conveniently elicited by performing a Fourier transform and studying the solutions from a spectral perspective.

For example, the discrete nonlinear Schrödinger equation appears in nonlinear optics and condensed matter physics, and its elliptic function solution for two oscillators is equivalent to nonlinear pendulum motion[4]. For two or three oscillators and a non-zero value of the nonlinearity parameter, its solution gives an infinite series of discrete spectral peaks[3]. Tracking their position and spacing as the nonlinearity parameter is changed yields interesting insights into the dynamical behaviour of the system.

In a similar vein, we shall be using Mathematica to generate spectral representations of firstly the nonlinear pendulum, and then the Lorenz equations, where we will be exploring such phenomena as the onset of chaotic behaviour.

2 Pendulum Motion

We illustrate our methods of analysis by studying the behaviour of the simple pendulum. Energy conservation considerations can be used to show that the equation of motion is

$$\ddot{\theta} + \omega_0^2 \sin\theta = 0, \tag{1}$$

where θ is the angular displacement, $\omega_0^2 = \frac{g}{l}$, g is the gravitational acceleration, l is the length of the pendulum, and a dot above a function indicates a time derivative.

In a brief survey of analytical solutions, we shall firstly consider the linearised equation, then a nonlinear solution due to Beléndez et al [1] that uses elliptic functions. Introducing our range of plotting

techniques, we shall generate numerical solutions with Mathematica and examine the salient features of the pendulum's behaviour.

2.1 Analytical Solutions

2.1.1 Linear Pendulum

For small oscillations, we can replace $\sin\theta$ in (1) with the leading order term in the Taylor expansion $\sin\theta \approx \theta + \frac{\theta^3}{3!} + \frac{\theta^5}{5!} + \ldots$ to obtain

$$\ddot{\theta} + \omega_0^2\theta = 0. \tag{2}$$

This linear second order differential equation has the general solution

$$\theta = A\cos(\omega_0\theta) + B\sin(\omega_0\theta) \tag{3}$$

where the constants A and B are determined by the initial conditions.

2.1.2 Nonlinear Pendulum

Beléndez et al obtained an exact solution to (1) using the Jacobi elliptic function $\mathrm{sn}(u;k)$. For a pendulum with initial conditions $\theta = \theta_0$ and $\frac{\mathrm{d}\theta}{\mathrm{d}t} = 0$ at $t = 0$, this was shown to be

$$\theta = 2\arcsin\left\{\sin\left(\frac{\theta_0}{2}\right)\mathrm{sn}\left[K\left(\sin^2\frac{\theta_0}{2}\right) - \omega_0 t; \sin^2\left(\frac{\theta_0}{2}\right)\right]\right\}, \tag{4}$$

where $K(m)$, the complete elliptical integral of the first kind, is defined as

$$K(m) = \int_0^1 \frac{\mathrm{d}z}{\sqrt{(1-z^2)(1-mz^2)}}. \tag{5}$$

Up to initial displacements of $\frac{3\pi}{4}$, this motion is similar to that of a simple harmonic oscillator with a modified angular frequency

$$\omega(\theta_0) = \frac{\pi\omega_0}{2K\left(\sin^2\left(\frac{\theta_0}{2}\right)\right)}. \tag{6}$$

2.2 Mathematica Plots

The behaviour of the nonlinear pendulum can be investigated by solving equation (1) numerically using Mathematica. We represent the results graphically using time-domain, phase, spectral and density plots.

2.2.1 Time Domain

Figure 1 shows the time dependence of the pendulum position for various values of the initial displacement θ_0. The pendulum oscil-

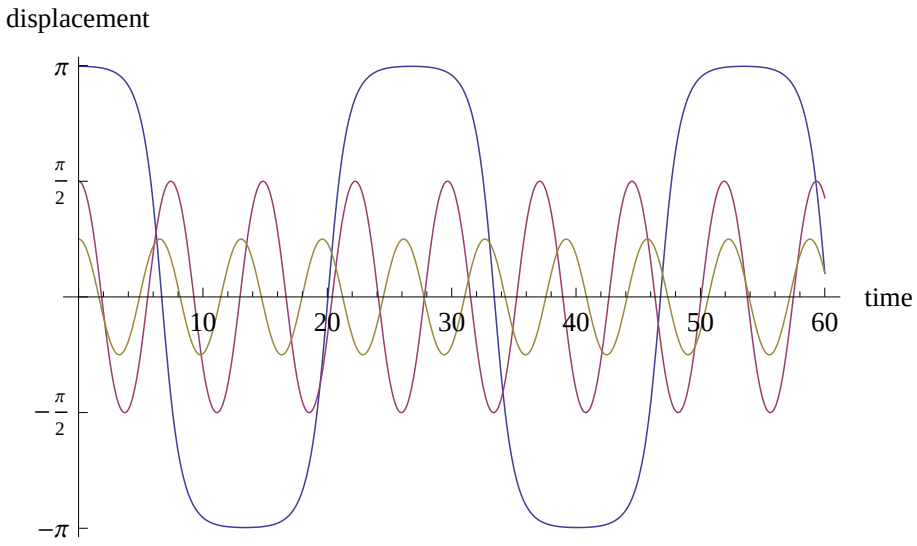

Figure 1: Evolution of displacement θ with time for simple pendula with initial displacements $\theta_0 = \pi - 0.01$, $\theta_0 = \frac{\pi}{2}$ and $\theta_0 = \frac{\pi}{4}$.

lations for $\theta_0 = \frac{\pi}{2}$ are larger and longer than for $\theta_0 = \frac{\pi}{4}$. When $\theta_0 = \pi - 0.01$, so that the pendulum is initially pointing almost vertically upwards, the time taken to complete these large-amplitude swings is much longer, and the pendulum pauses at $\pi - 0.01$ and $\pi + 0.01$.

2.2.2 Phase Portrait

The relationship between the pendulum's initial angular displacement and its motion can be seen clearly on a phase portrait. The pendulum equation (1) can be separated to give

$$\dot{\theta} = y, \quad \dot{y} = -\omega_0^2 \sin\theta. \tag{7}$$

Figure 2 shows trajectories on the $(\theta, \dot{\theta})$ plane for various starting positions. This phase portrait shows both oscillatory and rotational motion. An oscillating pendulum with an initial position in the interval $0 < \theta_0 < \pi$ and zero initial velocity starts off hanging to the right. The velocity then becomes increasingly negative and the pendulum decreases in θ as it swings left. The velocity reaches a maximum at $\theta = 0$ and then the pendulum slows down under gravity, reaching a stop at $-\theta_0$. The pendulum then begins to swing right: the velocity becomes positive, reaching a maximum at $\theta = 0$ before decreasing until $\theta = \theta_0$ again. The lines outside the oscillations correspond to rotational motion, which occurs for initial velocities greater than zero for particular values of θ.

2.2.3 Spectral Plot

Another way to represent the motion of the pendulum is to plot the spectrum in the frequency domain. A function of time $h(t)$ is related to its counterpart $H(f)$ in the frequency domain by the Fourier transform and its inverse:

$$H(f) = \int_{-\infty}^{\infty} h(t) e^{2\pi i f t} \mathrm{d}t, \quad h(t) = \int_{-\infty}^{\infty} H(f) e^{2\pi i f t} \mathrm{d}f. \tag{8}$$

We have used Mathematica to solve the pendulum equation numerically, so that our $h(t)$ is given as a discrete set of data. We therefore use an algorithm called a Fast Fourier Transform, a numerical analogue of (8) to obtain another discrete data set in the frequency domain. When we use the term "amplitude" in a spectral context, we are referring to $H(f)$ in equation (8). In the case of the pendulum, as $\theta(t)$ is an even, real function of t, its Fourier transform will also be real and even.

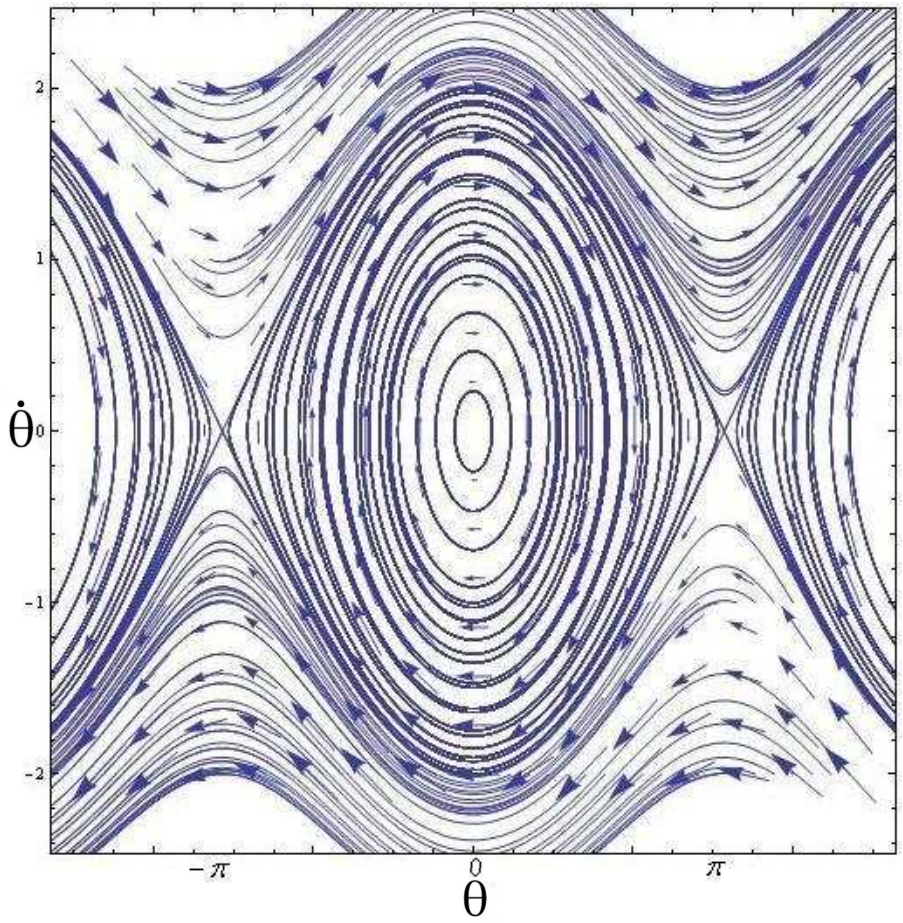

Figure 2: Phase space portrait of the pendulum angle θ plotted against angular velocity $\dot{\theta}$. The arrows indicate the direction of the trajectories.

Figures 3 and 4 show the spectral pictures of the pendulum motion for two different initial positions, $\theta_0 = \frac{\pi}{2}$ and $\theta_0 = \pi - 0.01$. Figure 3, for $\theta_0 = \frac{\pi}{2}$ has two large peaks at fairly low frequencies. The peaks are closer together in figure 4, for $\theta_0 = \pi - 0.01$, where we have already seen from the time-domain picture that the oscillations take longer. The maximum amplitudes are also seen to be higher in

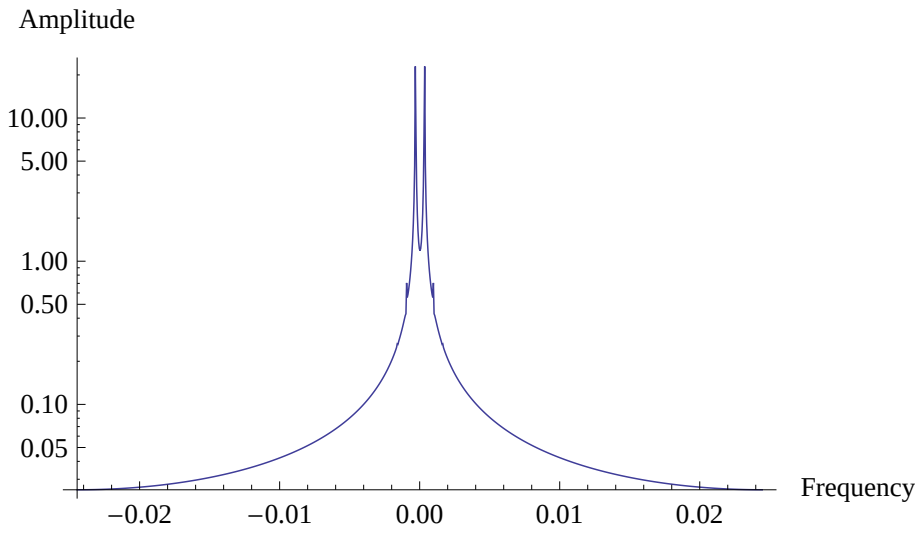

Figure 3: Spectral picture showing the relationship between the amplitude and frequency for a pendulum starting at $\theta = \frac{\pi}{2}$.

this case.

2.2.4 Density Plot

Figures 3 and 4 show the spectra for two different initial pendulum displacements. A qualitative picture of the spectra over the entire range of initial displacements θ_0 can be obtained using a spectral density plot, such as Figure 5. This shows 100 horizontal strips, corresponding to θ_0 being increased from zero to π. The amplitude is represented by shading, with lighter shades at frequencies where the amplitude is highest. For larger initial displacements, the peaks are closer to the zero frequency. In Section 2.2.1, the time-domain plots starting at larger displacements also exhibited longer periods of oscillation.

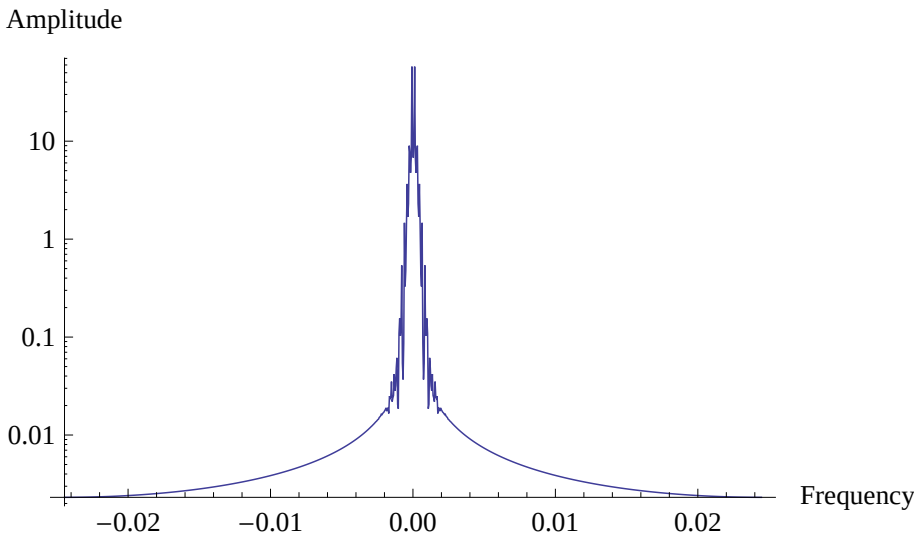

Figure 4: Spectral picture showing the relationship between the amplitude and frequency for a pendulum starting at $\theta = \pi - 0.01$.

3 The Lorenz System

3.1 Introduction

The Lorenz system [5] is a set of three nonlinear dimensional differential equations that was found to be extremely sensitive to small perturbations in the initial conditions, and to exhibit chaotic behaviour in certain circumstances. Lorenz, a meteorologist, derived the system

$$\dot{X} = -\sigma X + \sigma Y, \tag{9}$$

$$\dot{Y} = -XZ + rX - Y, \tag{10}$$

$$\dot{Z} = XY - bZ, \tag{11}$$

from a simplified form of the convection equations. The functions X, Y and Z were proportional to the intensity of convective motion, the temperature difference between the ascending and descending currents and the distortion of the vertical temperature from linearity.

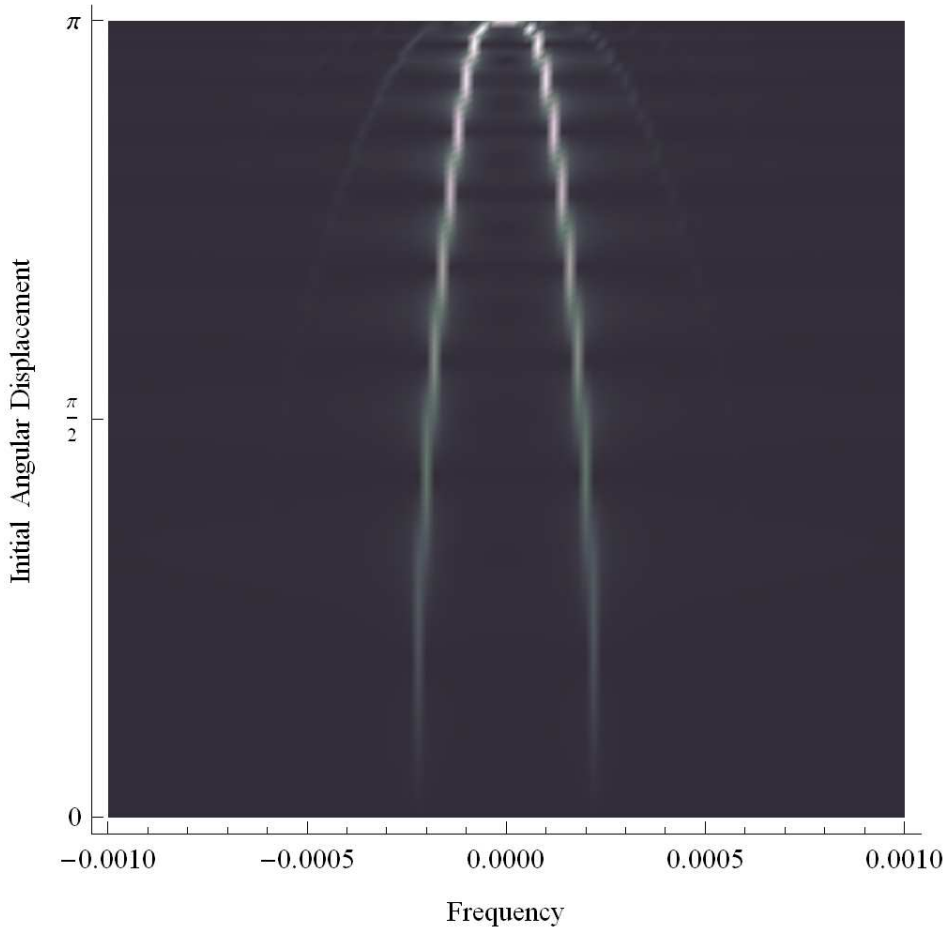

Figure 5: Density plot of 100 different spectra at varying initial displacements θ_0. Lighter greys represent higher amplitudes.

The constant σ is the Prantdl number, and b is a geometry parameter. We shall adopt the standard values of 10 and $\frac{8}{3}$, which are most commonly used to model the Earth's atmosphere. The parameter r is the Rayleigh number: if the Lorenz equations are being used to model a fluid, this determines the convective behaviour. We shall be varying this from zero to 30 to study its effect on the system.

While Lorenz obtained his differential system from fluid dynam-

ical equations, a number of other processes can also be modelled in this way. For example, the equations of motion for a damped pendulum rotating in the φ direction as well as the usual θ-direction can be written in the form (9)-(11) [2]. The spectral analysis of Section 3.3 shall be discussed in this context.

3.2 Fixed Points

Lorenz [5] analysed the fixed points of his system (9)-(11). These occur when $\dot{X} = \dot{Y} = \dot{Z} = 0$, and can hence be found by solving

$$0 = -\sigma X + \sigma Y, \tag{12}$$

$$0 = -XZ + rX - Y, \tag{13}$$

$$0 = XY - bZ. \tag{14}$$

A trivial solution to this is $(0, 0, 0)$. This is found to be a stable fixed point for $r < 1$, and unstable for $r > 1$.

Another solution is the pair of points $(\pm\sqrt{b(r-1)}, \pm\sqrt{b(r-1)}, r-1)$. These are only found when $r > 1$, as our functions X, Y and Z are real and the parameters b, σ and r are positive. These fixed points are stable when $r < r_B$, where

$$r_B = \frac{\sigma(\sigma + b + 3)}{\sigma - b - 1}, \tag{15}$$

and unstable when $r > r_B$.

Thus, as the Rayleigh number r is increased from zero, the system is expected to change considerably. At $r = 1$, the two other, stable fixed points appear, and the trivial fixed point becomes unstable. This is associated with the onset of convection. Then, at $r = r_B$ the pair of new fixed points become unstable. A bifurcation diagram of the X-axis and r will therefore have a pitchfork bifurcation at $r = 1$ where the two fixed points appear at $X = \pm\sqrt{b(r-1)}$. There will then be a subcritical Hopf bifurcation at $r = r_B$. The properties of the system as r is varied will be explored further in the next section.

3.3 Spectral Analysis

We can now use Mathematica to repeat the spectral analysis of Sections 2.2.3 and 2.2.4 for the Lorenz system. We obtain numerical solutions to the Lorenz equations (9)-(11) for $b = \frac{8}{3}$ and $\sigma = 10$. We then calculate $|\tilde{X}(f)|$, the magnitude of the Fourier transform of $X(t)$. As with the pendulum, we can plot spectra for individual values of the Rayleigh number r, or form a qualitative picture of the variation of the spectra over a range of r with spectral density plots.

Figure 6 shows a spectral density plot for the entire range of Rayleigh numbers considered. Each horizontal strip represents a spectrum at the appropriate r. Within each spectrum, the frequencies at which $|\tilde{X}(f)|$ is the highest are shown in the lightest shades. At $r = 1$, the onset of convection, there is a single, narrow peak with little noise. This region has the greatest contrast between the light central peak and the much darker surrounding area. A cross-section of the density plot of Figure 6 at $r = 1$ is plotted in Figure 7. This spectral plot resembles those in Section 2.2.3, and shows a single peak close to zero frequency, and no smaller peaks. However, these spectra have been generated from discrete numerical data, with a resolution reflecting the time duration of the sampling. There may in fact be two peaks, too close together to discriminate between without higher resolutions. If the Lorenz system (9)-(11) were modelling a pendulum, as in [2], the behaviour at $r = 1$ would correspond to extremely long-period oscillations with minimal damping.

Smaller peaks begin to develop as r increases above unity. In Figure 8, which shows the spectral densities for r up to 3.5, a pair of smaller-amplitude peaks form at either side of the large central peak and spread out to higher frequencies as r increases. For the pendulum, these indicate damping. In Figures 9-11, we can see the effect of this damping from spectral, time-domain and phase-space perspectives when $r = 3$. The system is attracted to the fixed point $(\sqrt{b(r-1)}, \sqrt{b(r-1)}, r-1)$, which is stable for low r.

Figure 12 shows the change in the spectra as r is increased from

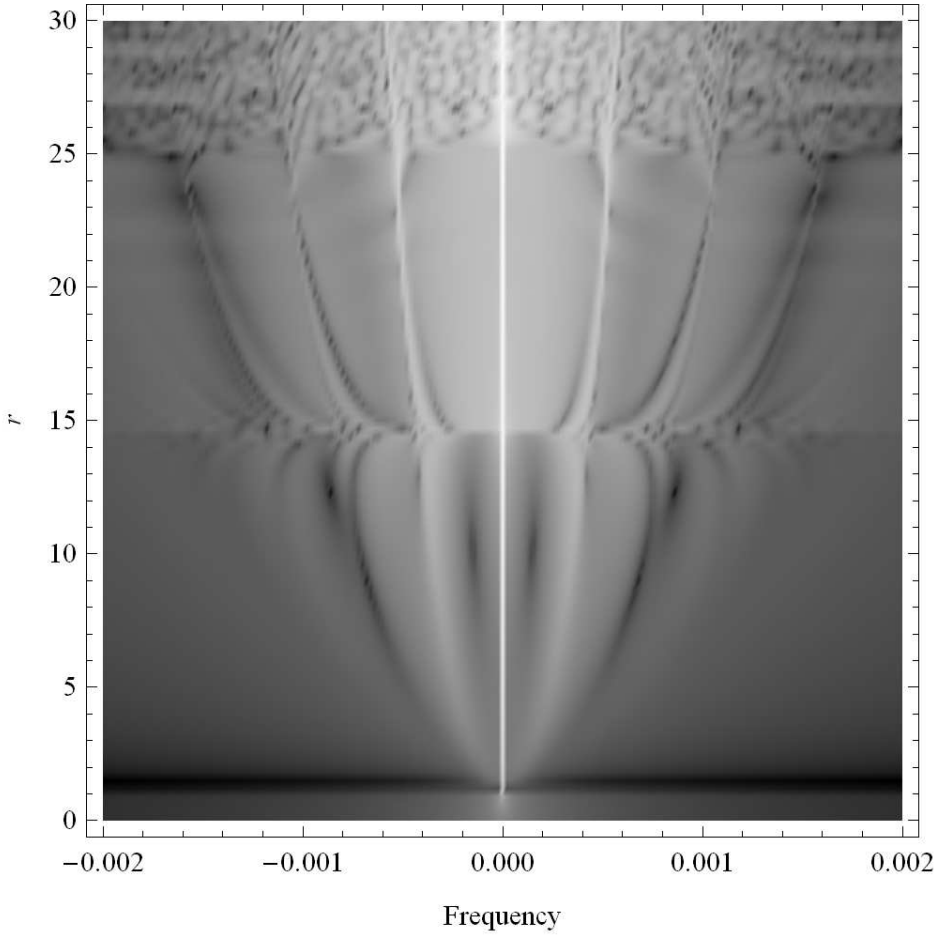

Figure 6: Spectral density plot for Rayleigh numbers varied from 0 to 30. Lighter greys represent higher amplitudes.

12 to 18. At the lower end of this scale, the system exhibits oscillatory behaviour with damping, although there are more small-amplitude peaks than observed in Figure 8. Sample spectral, time-domain and phase-space pictures for $r = 13$ are shown in Figures 13-15. Again, the trajectories approach the stable fixed point $(\sqrt{b(r-1)}, \sqrt{b(r-1)}, r-1)$.

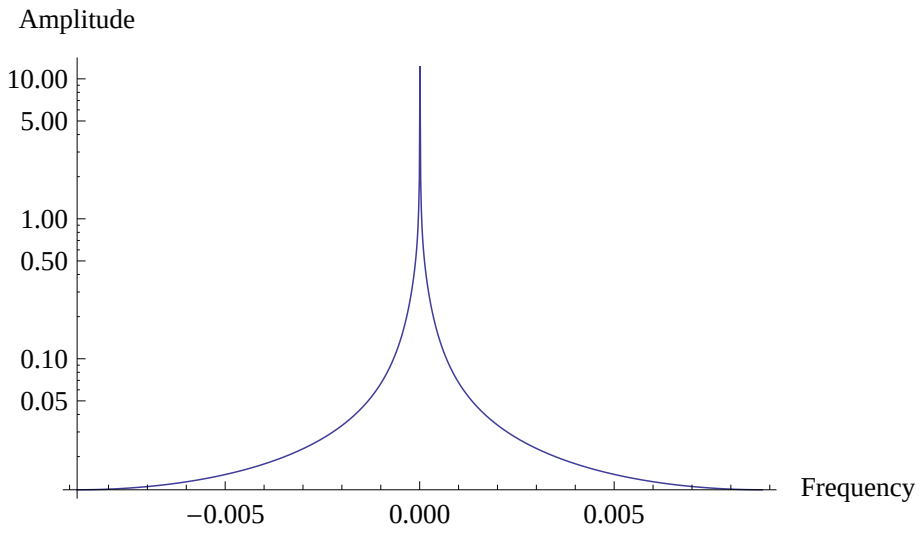

Figure 7: Spectral picture at $r = 1$, the onset of convection.

As r increases towards approximately 14, the level of damping is reduced, and Figure 12 shows an increase in the small-amplitude peaks. Between $r = 14$ and $r = 16$, noise can be observed in the spectra.

An unstable limit cycle appears at $r = 14.5463$. In Figure 12, the amount of noise increases markedly around this value of r. The limit cycle is examined in more detail in Figures 16-18. The value of $X(t)$ is seen to oscillate without any damping effects then comes out of this state and approaches the fixed point $(-\sqrt{b(r-1)}, -\sqrt{b(r-1)}, r-1)$. From the phase portrait in Figure 18, we can infer that a pendulum would oscillate much like the simple pendulum during the unstable limit cycle, then perform one full rotation as the phase trajectory crosses the fixed point $(0, 0, 0)$, before stabilising and performing damped oscillations.

Above $r = 15.5$ the chaotic behaviour diminishes. The spectrum in Figure 12 shows fewer, small-amplitude peaks than the chaotic zone, but spread out over a larger frequency range than the pure oscillatory stage. A pendulum would perform one rotation followed

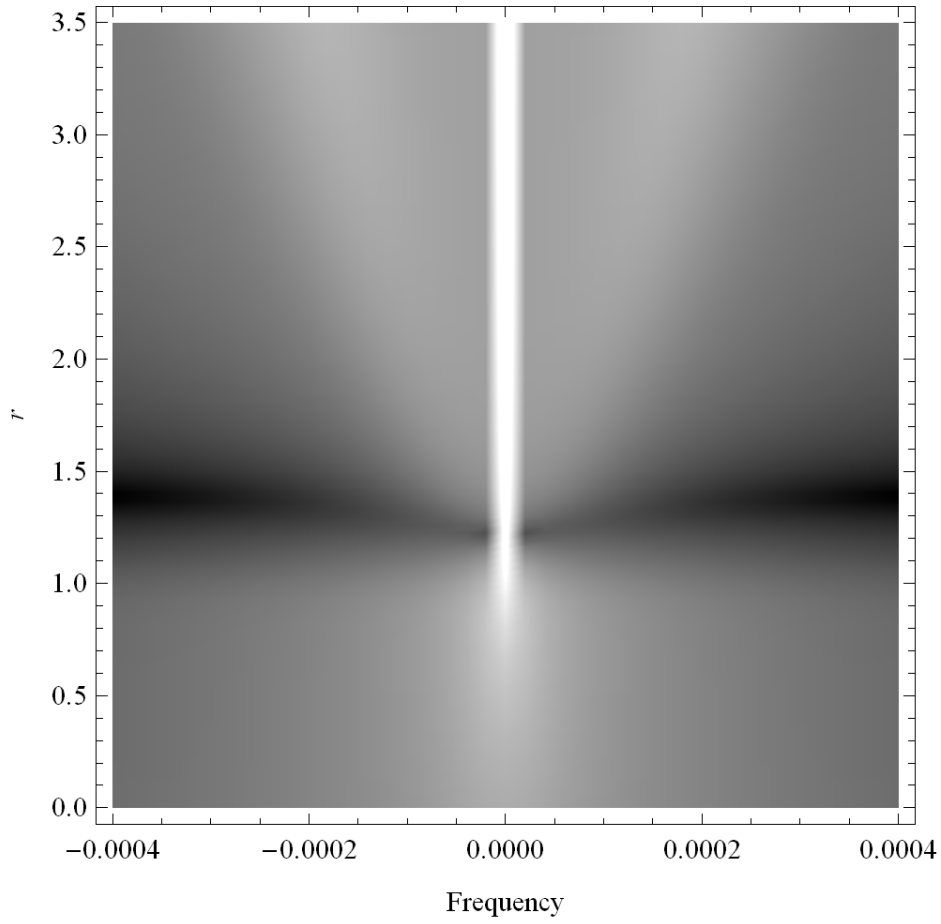

Figure 8: Spectral density plot for Rayleigh numbers varied from 0 to 3.5. A light pair of smaller-amplitude peaks appears at either side of the brighter central peak.

by damped oscillations.

Lorenz identified the onset of instability of convection with the Rayleigh number r_B given by equation (15), which, for our values of σ and b, is $\frac{470}{19}(\sim 24.74)$. This is borne out by the increase in noise after approximately this value of r in Figure 19. The chaotic behaviour continues up to $r = 30$, the highest value considered.

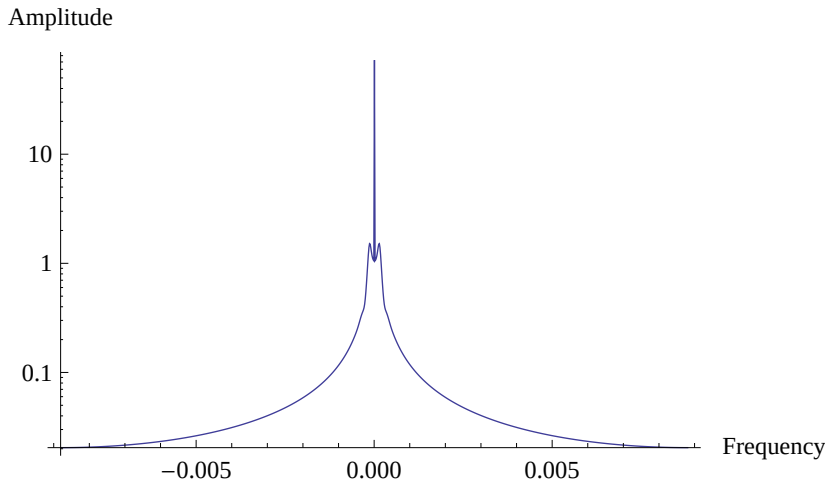

Figure 9: Spectral portrait for $r = 3$. Small additional peaks appear on either side of the central peak.

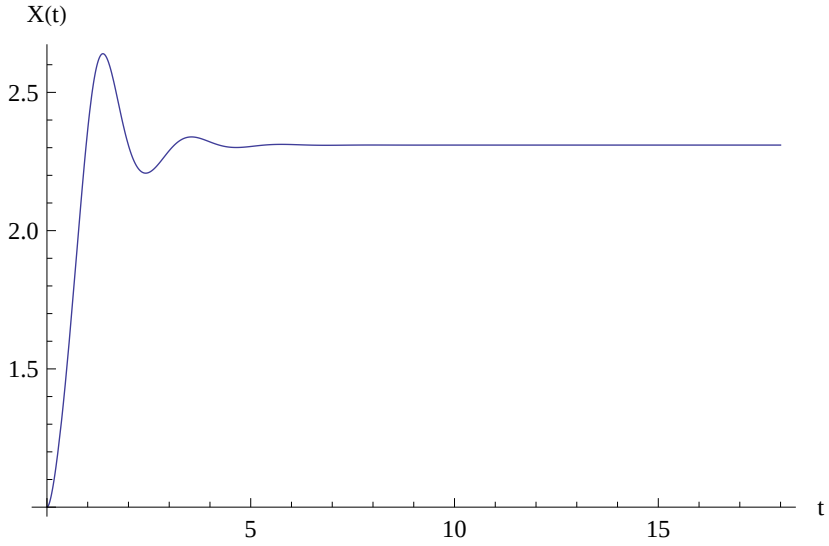

Figure 10: Time-domain plot of $X(t)$ for $r = 3$, showing rapid damping.

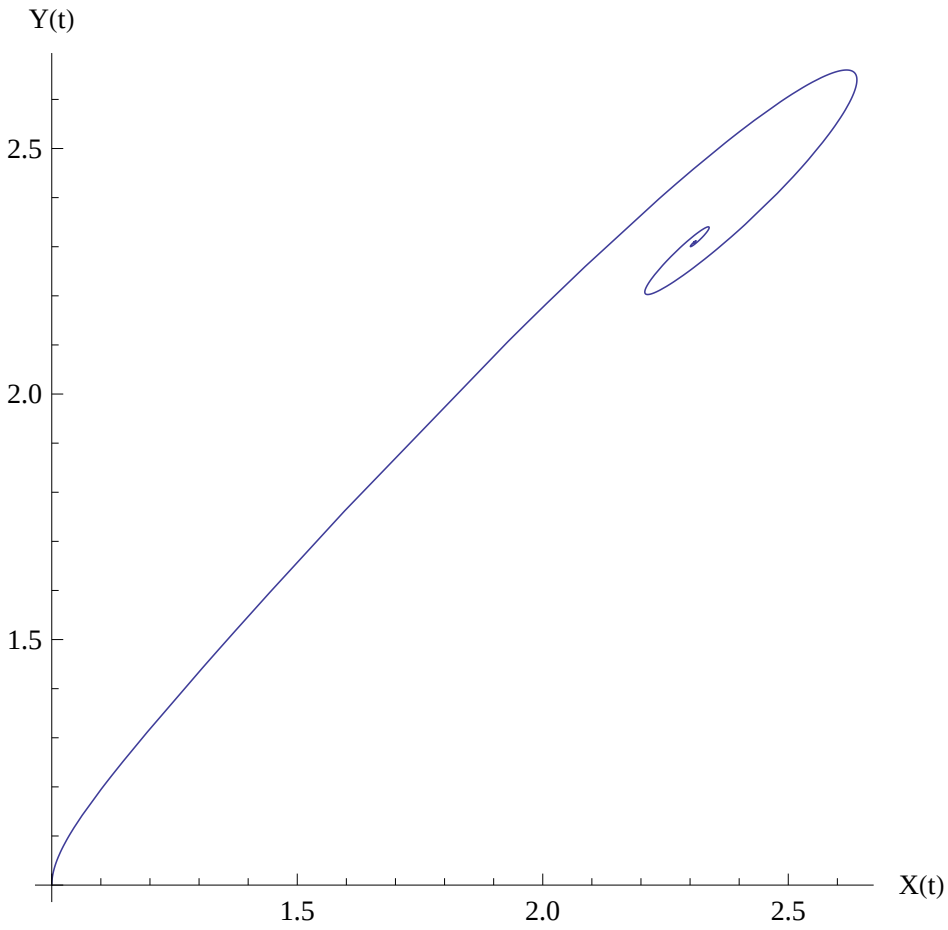

Figure 11: Phase portrait for $r = 3$, showing the trajectory in the (X, Y) plane. The system moves fairly directly towards the stable fixed point.

The data was sampled in the time domain up to $t = 18$. For Rayleigh numbers where the system is performing damped oscillations, the motion has died away by this time, so that the the spectra will not change if a larger time period is used. However, for $24.74 < r < 30$, the aperiodic motion persists and the precise spectra obtained will depend on the sampling time.

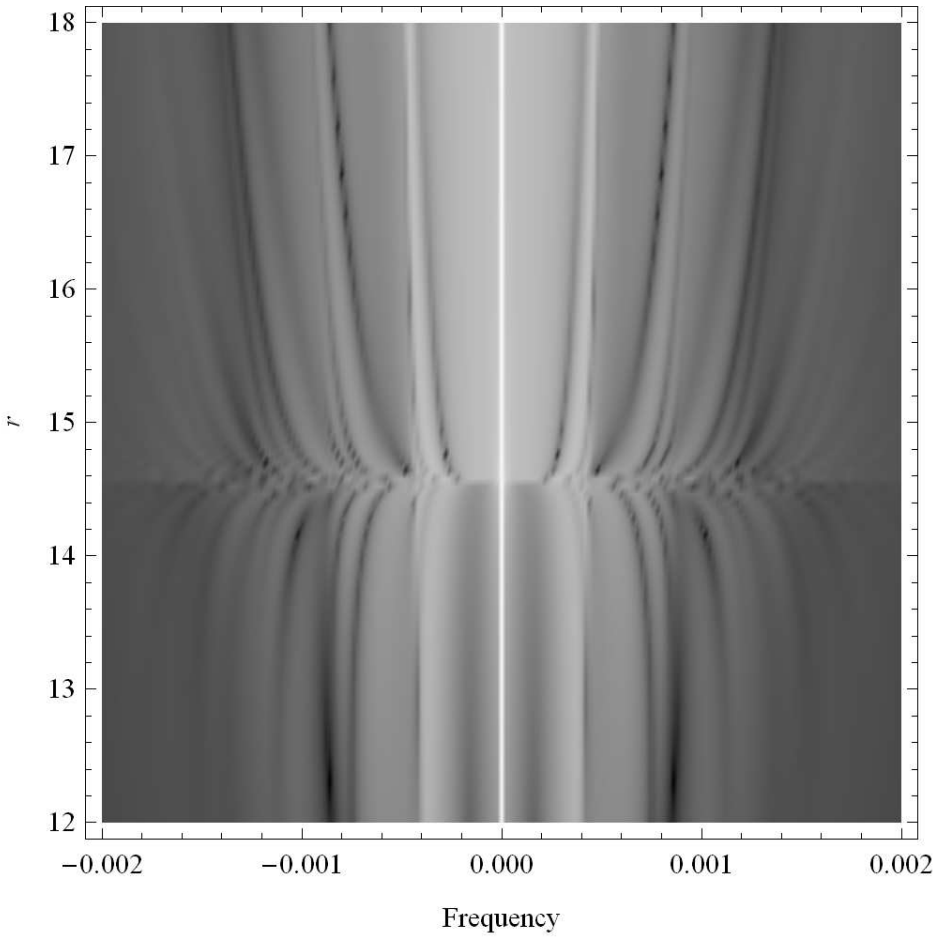

Figure 12: Spectral density plot for Rayleigh numbers varied from 12 to 18. Around the Noise begins to appear at $r = 14$ and continues until $r = 16$. It increases markedly around the limit cycle at $r = 14.5463$.

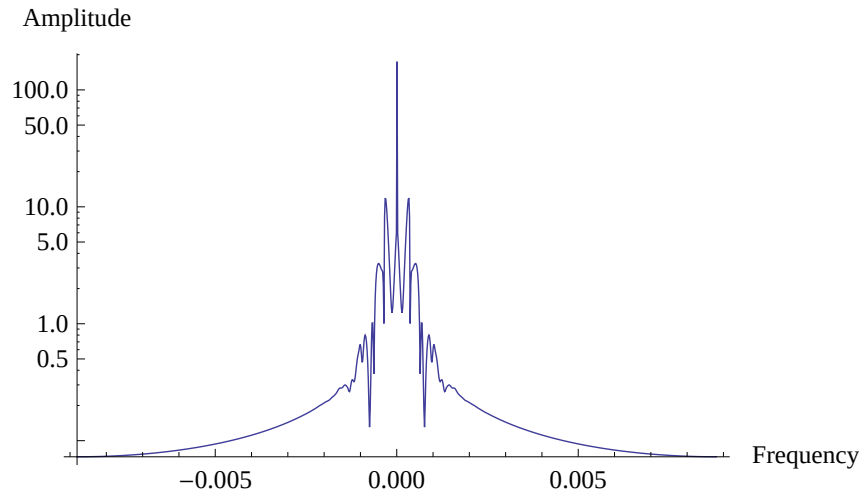

Figure 13: Spectral portrait for $r = 13$. The plot is more complex than Figure 9 for $r = 3$.

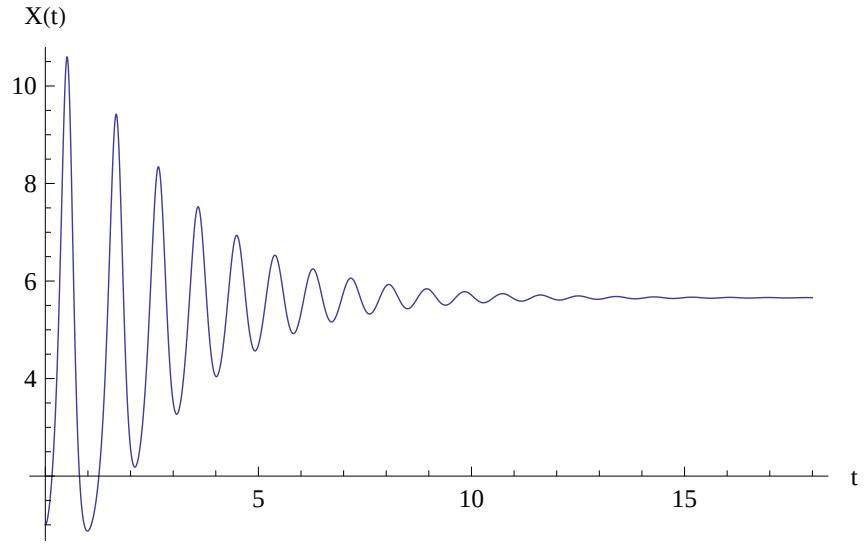

Figure 14: Time-domain plot of $X(t)$ for $r = 13$. The damping is more gradual than in Figure 10, allowing the system to perform more oscillations before it decays.

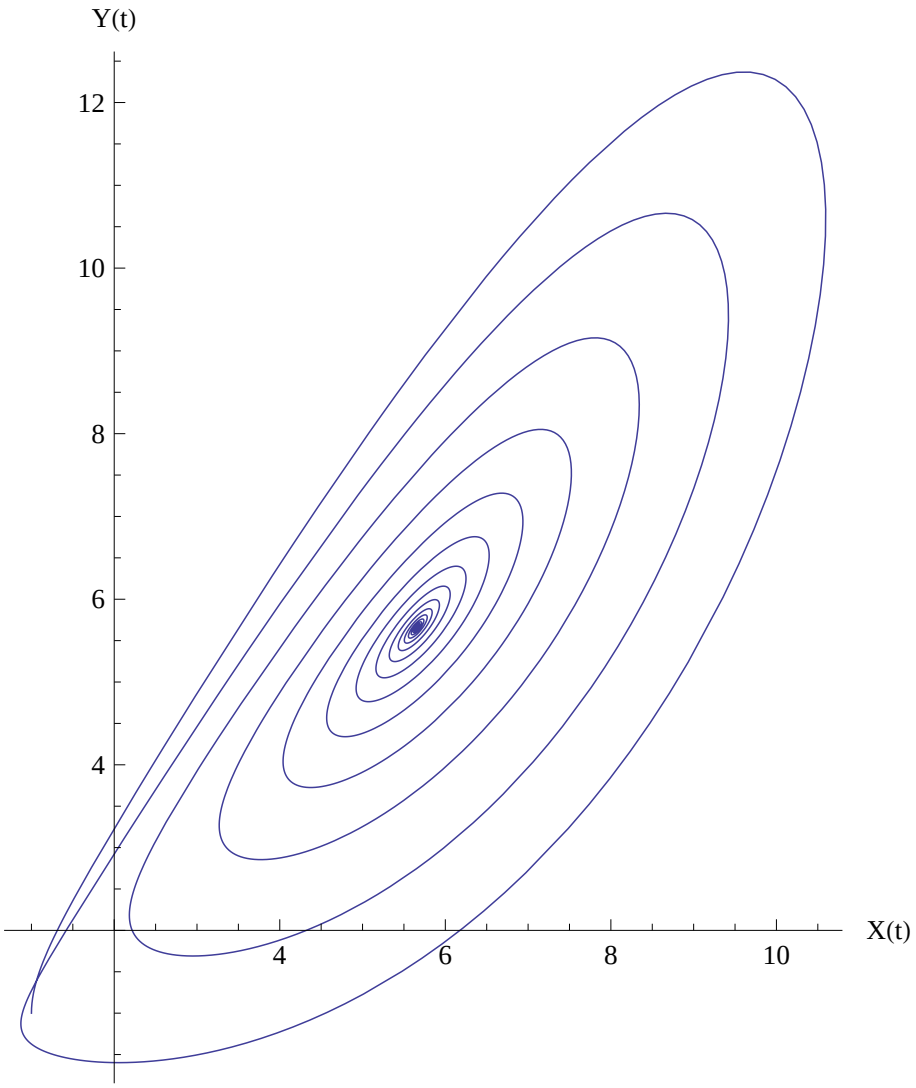

Figure 15: Spectral portrait for $r = 13$. The system oscillates around the fixed point several times before decaying.

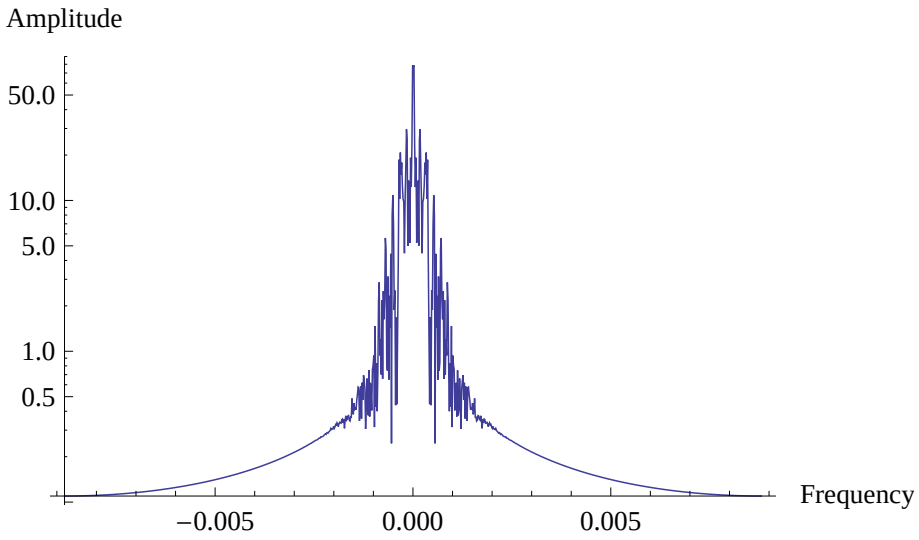

Figure 16: Spectral portrait for $r = 14.5463$, showing a lot of noise.

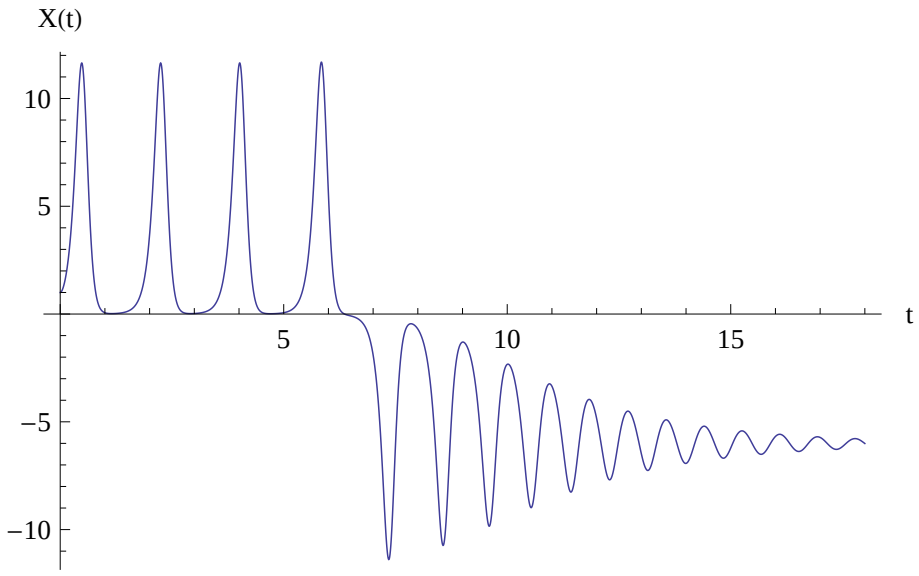

Figure 17: Time-domain plot of $X(t)$ for $r = 14.5463$, showing an unstable limit cycle. The system oscillates without damping, then crosses the X axis and decays to a stable fixed point.

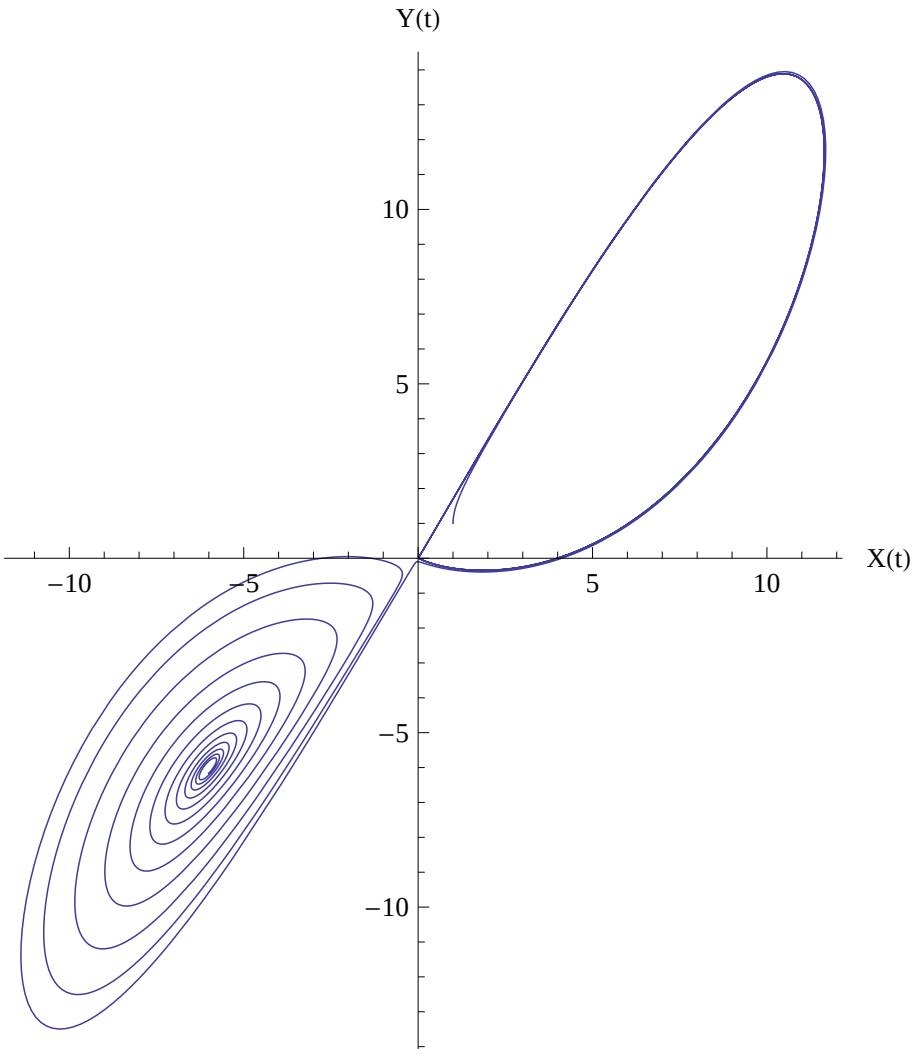

Figure 18: Phase portrait for $r = 14.5463$. The system leaves an unstable limit cycle in the first quadrant to eventually decay to a stable fixed point in the third quadrant.

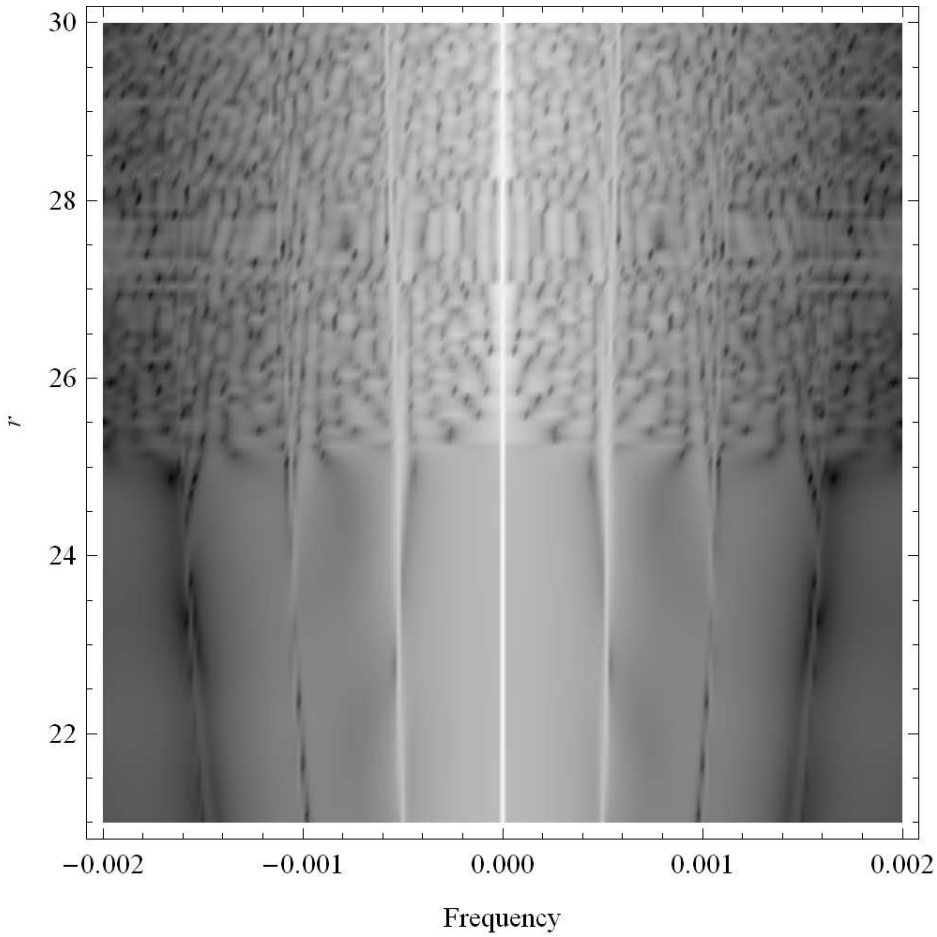

Figure 19: Spectral density plot for Rayleigh numbers varied from 21 to 30. The peaks in the bottom half indicate one rotation followed by damped oscillation for a pendulum. The top half shows chaotic behaviour.

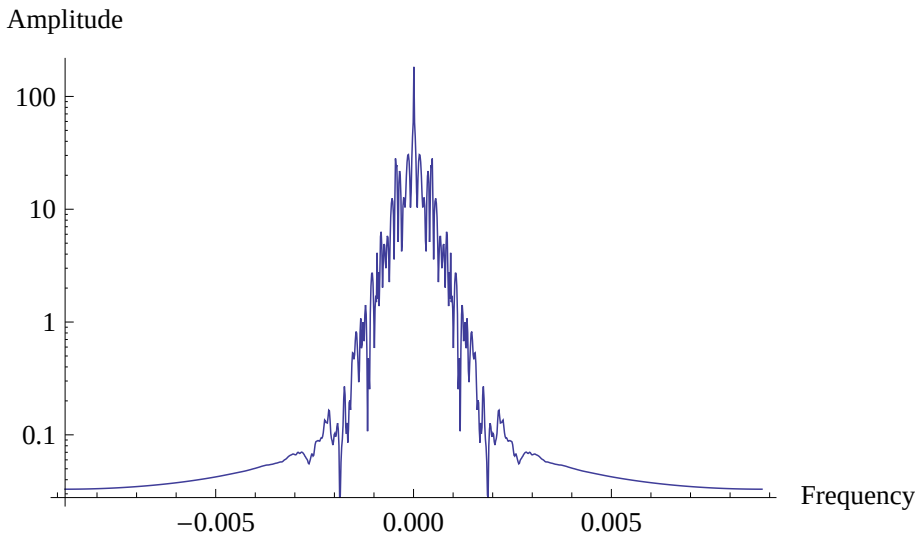

Figure 20: Spectral portrait for $r = 26$, when the system is exhibiting chaotic behaviour.

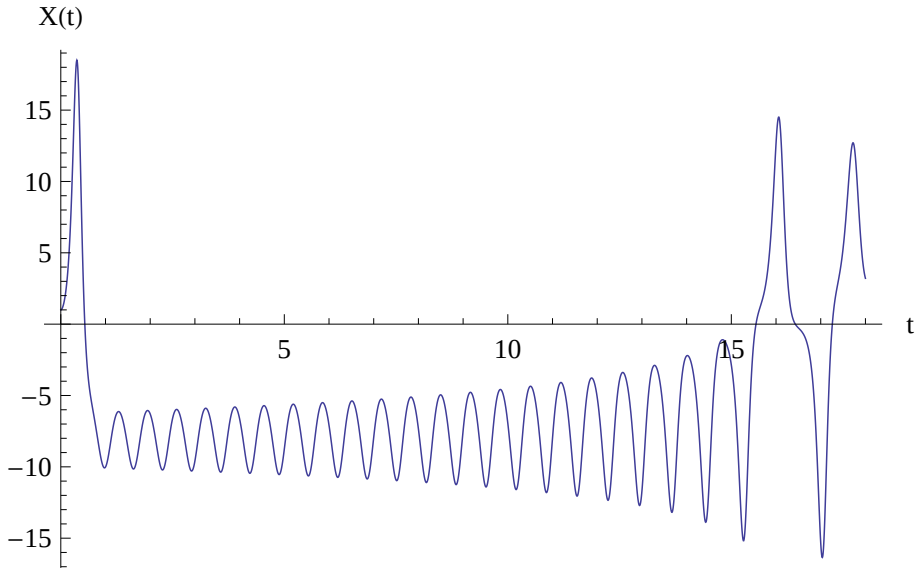

Figure 21: Time-domain portrait of $X(t)$ for $r = 26$, when the system is exhibiting chaotic behaviour.

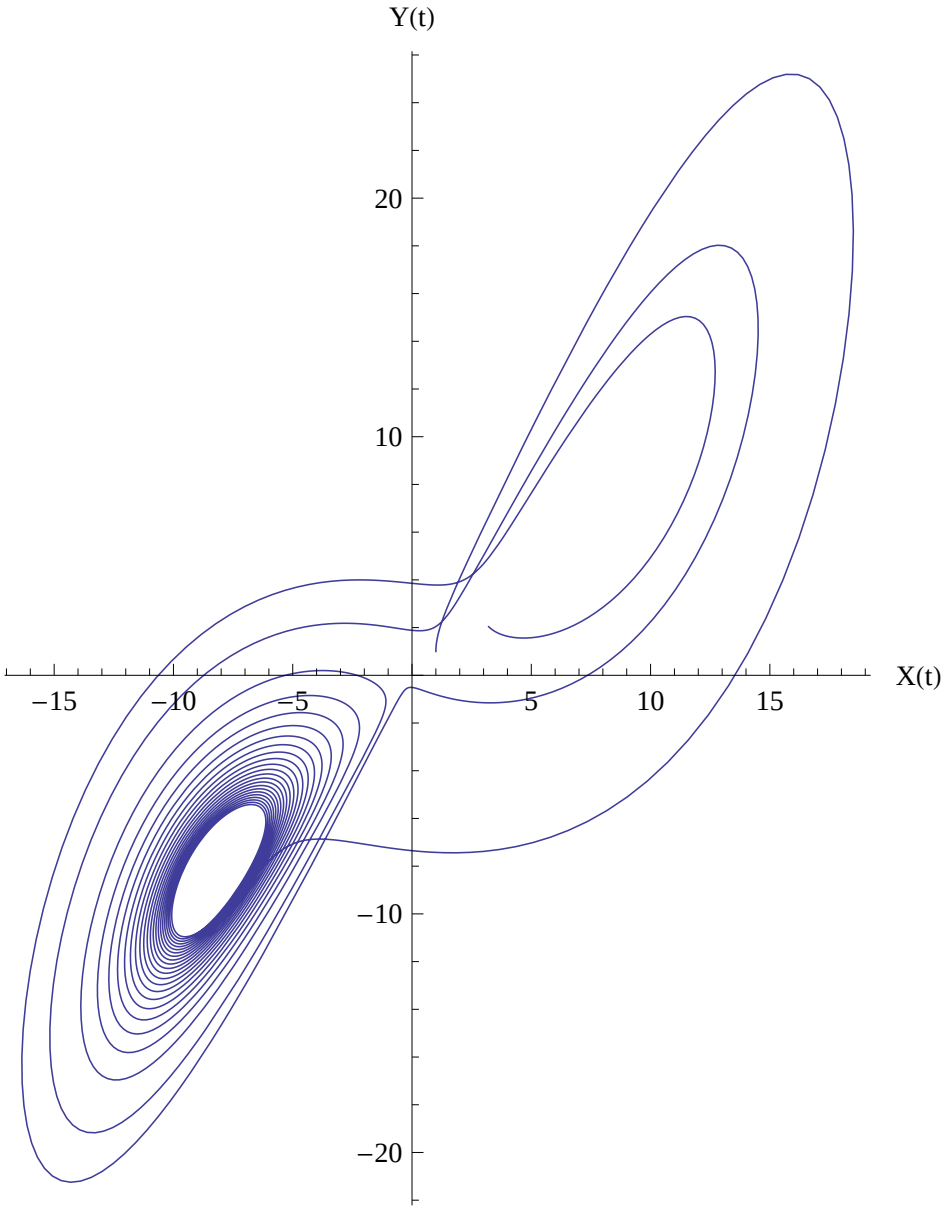

Figure 22: Phase portrait for $r = 26$, when the system is exhibiting chaotic behaviour.

Figures 20-22 show an example of such chaotic behaviour.

The time domain plot shows a peak around $t = 17$, where X moves towards the positive fixed point, then drops back towards the negative one. This trend continues for an infinite time and does not converge to a fixed point. The fixed points in the phase plane are no longer stable or unstable, and the trajectories wander between them in an unpredictable way, moving around one and then circling back to the other. The time spent reaching an attractor may be infinite, in which case it is known as a strange attractor. In this chaotic region, the motion of a pendulum becomes an unpredictable mixture of rotations and oscillations.

4 Conclusion

The Fourier domain is a useful arena in which to study the dynamics of nonlinear systems. Spectral density plots are well suited to observing the changes to a system as one of the parameter is varied. In this way, we were able to observe the dependence of the period of a pendulum's motion on its the starting displacement. Similarly, the spectral perspective offers useful insights into the Lorenz system, which exhibits dramatically different behaviour as the Rayleigh number r is changed. Frequency spectra complement the time domain plots and phase portraits, leading to a more complete picture of the system in regimes such as convection and chaotic motion. The spectral density plots showed the system shifting from one state to the other as r is increased, and confirmed Lorenz's values for the onset of convection and chaos.

Acknowledgements

This research was carried out with support from the UHI Strategic Development Body, the European Regional Development Fund, Highlands and Islands Enterprise and Comhairle nan Eilean Siar.

References

[1] Beléndez A, Pascual C, Méndez D I, Beléndez T, Neipp C, Exact solution for the nonlinear pendulum, *Rev. Bras. Ensino Fs.* 29,4 (2007) 645-648

[2] Clerc M, Coullet P, Tirapegui E, Lorenz Bifurcation: Instabilities in Quasireversible Systems, *Phys. Rev. Lett.* , 83, 19, (1999), 3820-3823.

[3] Finlayson N, Blow K J, Hamiltonian chaos in the Discrete Nonlinear Schrodinger Equation, *Chaos, Solitons and Fractals* 8/9 (1994) 1817-1834

[4] Jensen S, The nonlinear coherent coupler, *IEEE Journal of Quantum Electronics* 18, 10, (1982), 1580-1583

[5] Lorenz E N, Deterministic nonperiodic flow, *Journal of the Atmospheric Sciences*, 20, (1963) , 130-141.

[6] Xu, Xu *"Nonlinear Dynamics of Parametric Pendulum for Wave Energy Extraction"* Ph.D. Thesis, Aberdeen University, 2005.

Submitted on December 2009, revised on May 2010.

Spektralna analiza nelinearnih sistema

Proučena su dva razdvojena nelinearna diferencijalna sistema u frekventnom i vremenskom domenu korišćenjem crteža generisanih kodom Mathematica. Crteži spektralne gustine su posebno interesantni jer mogu da podesno pokažu efekat promene jedog od parametara sistema. Na ovaj način su posmatrani uticaji početnog pomeranja na nelinearno klatno kao i ponašanje Lorencovog sistema pri promeni Rejlijevog broja.

doi:10.2298/TAM1002111B Math.Subj.Class.: 34C15, 34D45